Solid-state optical properties of linear polyconjugated molecules: π-stack contra herringbone

Johannes Gierschner[a)]
Laboratory for Chemistry of Novel Materials, Center for Research in Molecular Electronics and Photonics, University of Mons-Hainaut, Place du Parc 20, B-7000 Mons, Belgium and Institute for Physical and Theoretical Chemistry, University of Tübingen, Auf der Morgenstelle 8, 72076 Tübingen, Germany

Markus Ehni
Institute for Physical and Theoretical Chemistry, University of Tübingen, Auf der Morgenstelle 8, 72076 Tübingen, Germany

Hans-Joachim Egelhaaf
Institute for Physical and Theoretical Chemistry, University of Tübingen, Auf der Morgenstelle 8, 72076 Tübingen, Germany and Dipartimento di Fisica, Politecnico di Milano, Piazza Leonardo da Vinci, 32, 20133 Milano, Italy

Begoña Milián Medina and David Beljonne
Laboratory for Chemistry of Novel Materials, Center for Research in Molecular Electronics and Photonics, University of Mons-Hainaut, Place du Parc 20, B-7000 Mons, Belgium

Hadjar Benmansour and Guillermo C. Bazan
Department of Chemistry, University of California, Santa Barbara, California 93106

(Received 15 June 2005; accepted 18 August 2005; published online 12 October 2005)

The intermolecular arrangement in the solid state and the consequences on the optical and photophysical properties are studied on different derivatives of oligophenylenevinylenes by UV/VIS absorption and angular-resolved polarized fluorescence spectroscopy. Unsubstituted distyrylbenzene (DSB) organizes in a herringbone manner, with the long axes of the molecules oriented in parallel, but the short axes almost perpendicular to each other. Fluorinated distyrylbenzene (F_{12}DSB) as well as the DSB:F_{12}DSB cocrystals prefer cofacial π-stacking in the solid state. For all structures, the consequence of the parallel alignment of the transition moments is a strongly blueshifted H-type absorption spectrum and a low radiative rate constant k_F. Significant differences are observed for the emission spectra: the perpendicular arrangement of the short axes in DSB crystals leads to only very weak *intermolecular* vibronic coupling. Hence the emission spectrum is well structured, very similar to the one in solution. For F_{12}DSB and DSB:F_{12}DSB, the cofacial arrangement of the adjacent molecules enables strong intermolecular vibronic coupling of adjacent molecules. Thus, an unstructured and strongly redshifted excimerlike emission spectrum is observed. The differences in the electronic nature of the excited states are highlighted by quantum-chemical calculations, revealing the contribution of interchain excitations to the electronic transitions. © *2005 American Institute of Physics*. [DOI: 10.1063/1.2062028]

I. INTRODUCTION

Polymeric and oligomeric π-conjugated organic molecules based, e.g., on phenylenevinylene, thiophene, or acene repetition units are widely investigated materials as active layers for optoelectronic devices. The optical and photophysical properties of these materials are not only influenced by the chemical structure of the molecules (backbone and substitution pattern) but to a large extent by the intermolecular organization. Regular packing of the molecules is often based either on a herringbone arrangement or on a cofacial π-stack of adjacent molecules. The way of packing might have a significant impact on the nature and dynamics of energy and charge carriers in these materials, which is a challenging issue in the rational design of organic light-emitting diodes, solar cells, and field-effect transistors.

Here we report on two model oligophenylenevinylene (OPV) compounds for which single crystals have been grown and their x-ray structures were determined: unsubstituted distyrylbenzene, DSB,[1] and a fluorinated species, F_{12}DSB (Ref. 2) (see Fig. 1). DSB adapts the well-known herringbone structure in the solid state, which is also found for other unsubstituted rod-shaped OPVs,[3] polyphenylenevinylene (PPV),[4] and oligothiophenes,[5] -phenylenes,[6] and -acenes.[7] Fluorination of DSB modifies significantly the electrostatic potential of the molecule, shifting the electron density from the carbon backbone to the periphery.[2] The changes in the electrostatic distribution induces a change in the solid-state arrangement due to interactions of the local carbon-fluorine dipole moments,[8,9] so that F_{12}DSB crystallizes in layers of slightly shifted cofacially oriented molecules, i.e., π-stacks.[2] A very similar packing is observed for the 1:1 cocrystal of DSB:F_{12}DSB.[10] Cofacial arrangements

[a)]Electronic mail: johannes@averell.umh.ac.be

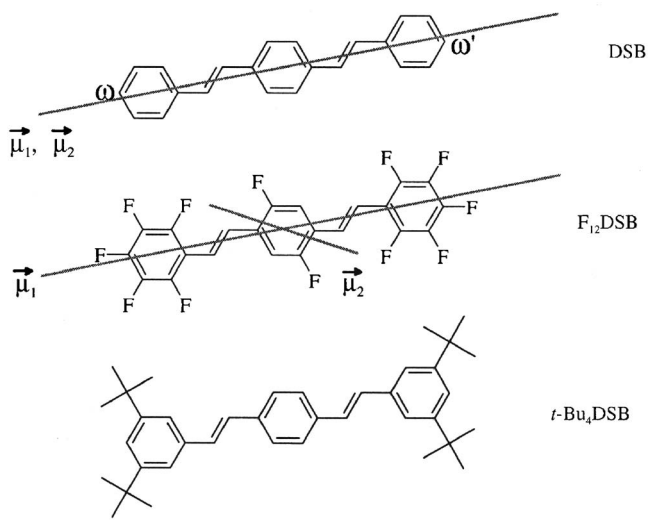

FIG. 1. Unsubstituted (DSB), fluorosubstituted (F_{12}DSB), and *t*-butyl-substituted distyrylbenzene (*t*-Bu_4DSB). The direction of the $\mu_1(1A_g \rightarrow 1B_u)$ and $\mu_2(1A_g \rightarrow 2B_u)$ transition dipole moments are shown as gray lines.

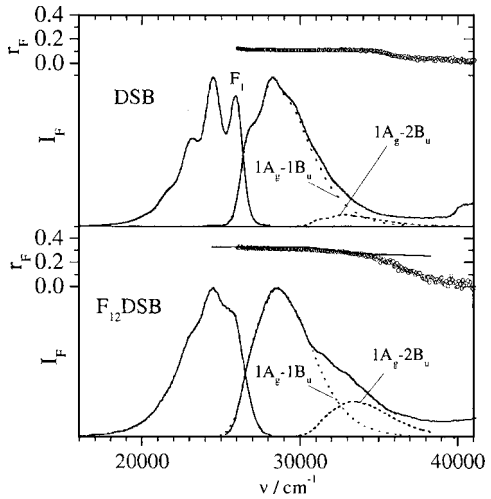

FIG. 2. Fluorescence emission (left) and excitation spectra (right) of DSB in PDMS (solid lines, top) and F_{12}DSB in PFMS (solid lines, bottom). Dotted lines: simulated $1A_g \rightarrow 1B_u$ absorption spectra (see text). Dashed lines: simulated $1A_g \rightarrow 2B_u$ absorption spectra. Open symbols: fluorescence excitation anisotropy r_F recorded at λ_{em}=440 nm.

are also found, for example, in pyrene and perylene single crystals,[11] however, in this case in order to promote dense packing.

In this paper we investigate the consequences of the different packing motifs of DSB, F_{12}DSB, and DSB:F_{12}DSB on the optical and photophysical properties by absorption and fluorescence spectroscopy under time- and angular-resolved, polarized conditions. The solid-state properties are studied on single crystals and on nanoparticle suspensions, which are readily prepared by the precipitation method.[12–15] The optical and photophysical properties of nanoparticles are very similar to those of thin vapor-deposited films, but in contrast to films, nanoparticle suspensions can be handled like solutions in spectroscopic experiments.[13]

The first part of the work describes the optical and photophysical properties in solution in order to understand the nature of the excited electronic states of the molecules without any interchromophore interaction. We then introduce isotropic intermolecular interactions, which are observed in condensed phases of *tert*-butyl-substituted DSB (*t*-Bu_4DSB, see Fig. 1), where the bulky substituents prevent long-range ordering of the molecules. We show how intermolecular orientations and interactions can be monitored with UV/VIS absorption and polarized fluorescence techniques. In the following, these techniques are applied to DSB, F_{12}DSB, and DSB:F_{12}DSB nanoparticles and single crystals, in order to establish structure-property relationships. The striking differences in the emission properties are discussed in terms of interchain excitations and intermolecular vibronic coupling.

II. EXPERIMENT

A. Materials and methods

DSB was synthesized according to the method of Siegrist *et al.*[16] and Erckel and Frühbeis.[17] The synthesis of fluorinated distyrylbenzene, F_{12}DSB, was described elsewhere.[2] *t*-Bu_4DSB was prepared by Schenk *et al.*[18] For fluorescence anisotropy measurements of solutions, DSB was dissolved in polydimethylsiloxane (PDMS, viscosity η=5000 cPoise) and F_{12}DSB was dissolved in poly(trifluoropropyl-methyl-siloxane) (PFMS, viscosity η =500 cPoise), with absorbancies $A<0.05$. Nanoparticle suspensions were prepared by fast precipitation from methanol solutions (concentration $c=2\times10^{-5}M$) by addition of water (methanol/water 1:4 v/v). The solutions and suspensions were measured in a right-angle geometry on a Spex Fluorolog 222 spectrofluorimeter. For polarized fluorescence measurements, the spectrometer was additionally equipped with Glan-Thompson polarizers for exciting and emitted light. Time-resolved fluorescence was recorded by the single-photon counting technique. For angular-resolved measurements on F_{12}DSB single crystals, the needle-shaped crystal was deposited on a fused silica slide. The silica slide was mounted on a turntable in such a way, that the long needle axis (crystal *c* axis) coincided with the vertical laboratory axis. The sample was rotated around the vertical axis, and the lateral position was adjusted for maximum fluorescence intensity at each rotation angle.

B. Computational details

The equilibrium geometries in the electronic ground and first excited states (S_0 and S_1), and the adiabatic and vertical transition energies were computed at the (time-dependent) density-functional B3LYP level of theory, assuming a planar geometry of the molecules' backbones (C_{2h} symmetry). For comparison, *ab initio* Hartree-Fock (HF) and restricted configuration singles (RCIS) calculations were performed. All density-functional theory (DFT) calculations were carried out using the TURBOMOLE 5.7.1 quantum-chemical package.[19] The HF and CIS calculations were performed with the GAUSSIAN 98 program code.[20] In all calculations the standard 6-311G* basis set was used.

Vertical transition energies and electron-hole two-particle wave functions of dimer pairs were obtained by the

TABLE I. Photophysical properties of DSB and F_{12}DSB in solution (cyclohexane) and in the solid state (nanoparticles).

		DSB		F_{12}DSB	
		Solution[a]	Solid state	Solution[a]	Solid state
Absorption maximum	ν_{abs}/cm^{-1}	28 600	33 900	28 500	35 500
Fluorescence maximum	ν_{em}/cm^{-1}	24 700	22 700	24 400	18 000
Fluorescence quantum yield	Φ_F	0.77	0.1	0.67	0.008
Fluorescence decay time	τ_F/ns	1.52	2.5[b]	1.52	8.3[c]
Radiative rate constant	k_F/ns^{-1}	0.51	0.04	0.44	0.001

[a]From Ref. 2.
[b]Mean decay time calculated from biexponential fit.
[c]Mean decay time calculated from three-exponential fit.

ZINDO/S (Zerner's spectroscopic parameterization for intermediate neglect of differential overlap for spectroscopy) method,[21] taking into account full single configuration interaction (SCI) over the occupied and unoccupied π-type molecular orbitals (MOs). The molecular geometries and orientations of the dimer pairs were taken from the x-ray structures.[2,10,22]

III. RESULTS AND DISCUSSION

A. Optical properties in solution

The absorption spectra of DSB, *t*-Bu_4DSB, and F_{12}DSB in solution are dominated by the $S_0(1A_g) \rightarrow S_1(1B_u)$ transition (see Fig. 2). According to polarized fluorescence studies on DSB in stretched polyethylene films,[14,23] the transition dipole moment $\mu(S_0 \rightarrow S_1)$ is oriented approximately parallel to the long geometrical axis of the molecule $d_{\omega\omega'}$ (see Fig. 1). The solutions exhibit intense fluorescence (Table I), originating from the electronically allowed $1A_g \leftarrow 1B_u$ transition. The vibronic fine structure of the emission and absorption spectra is well understood by the Franck-Condon (FC) activities of a_g in-plane C–C stretching and bending vibrational modes, preferentially located in the vinylene units. The emission spectra are better resolved than the absorption spectra due to the steeper torsional potential in the S_1 state.[24] The spectral positions *in vacuo*, which are the reference point for a comparison with quantum-chemical calculations, can be obtained by extrapolation of the spectral positions as a function of the polarizability of the solvent.[24] The spectral shifts are almost identical for all three compounds under study, see Table II, due to similar oscillator strengths and molecular shapes.

The introduction of substituents into the molecular backbone causes some subtle changes of the optical properties: the spectra are slightly redshifted against DSB by $-400\ cm^{-1}$ for *t*-Bu_4DSB and $-500\ cm^{-1}$ for F_{12}DSB, respectively. The pronounced shoulder in the absorption spectrum of F_{12}DSB, located at around $33\,000\ cm^{-1}$ (Fig. 2), is found only as a weak shoulder in the spectra of DSB and *t*-Bu_4DSB. Franck-Condon analysis of low-temperature spectra of DSB indicates that the shoulder belongs to a different electronic tran-

TABLE II. Experimental (expt.) and calculated (calc.) adiabatic and vertical electronic transition energies ($\times 1000\ cm^{-1}$). Calculated transition dipole moments: length (in Debye) and orientation γ against the long molecular axis (see Fig. 1) (in degrees). γ is defined as the angle between μ and $d_{\omega\omega'}$ (see Fig. 1).

				DSB	*t*-Bu_4DSB	F_{12}DSB
Adiabatic transition energy	$1A_g \rightarrow 1B_u$	Expt.	In *n*-hexane[a]	26.1	25.7	25.6
			in vacuo[b]	27.7	27.4	27.2
		Calc.	RCIS[c]	28.1	27.8	28.4
			DFT[d]	23.9	23.6	23.6
Energy difference	$2B_u \rightarrow 1B_u$	Expt.		4.5	4.5	4.8
		Calc.	DFT	9.0	8.2	6.3
Vertical transition energy	$1A_g \rightarrow 1B_u$	Expt.	*in vacuo*[e]	29.8	29.5	29.3
		Calc.	DFT	25.6	25.1	25.1
Transition dipole moment $1A_g \rightarrow 1B_u$	Length	μ	DFT	12.3	13.1	12.4
	Orientation	γ	DFT	2°	1°	2°

[a]In a first approximation the adiabatic transition energy can be identified with the F_1 position of the experimental spectrum, see Fig. 2 (Ref. 24).
[b]From extrapolation of the spectral positions in different solvents against the polarizability of the solvents according to the Onsager relation (Ref. 25).
[c]Basis set: 6-311G*.
[d]Time-dependent density functional B3LYP/6-311G*.
[e]From the adiabatic transition by addition of the equilibrium energy (Ref. 24).

sition, assigned to the $2B_u$ state. According to fluorescence anisotropy measurements of DSB in highly viscous media (Fig. 2), the $1A_g \rightarrow 2B_u$ band is polarized in the same direction as the $1A_g \rightarrow 1B_u$ transition. The relative contributions of both transitions to the main absorption band can be determined with the help of the emission spectrum, if the molecular geometries as well as the normal coordinates of the a_g vibrational modes are not very different in the $1A_g$ and the $1B_u$ state, which is the case for DSB-based molecules.[24] Then, the emission spectrum can be mirrored at the spectral origin and convoluted with an exponential distribution function, accounting for the steeper torsional potential in the $1B_u$ state.[24] The resulting $1A_g \rightarrow 1B_u$ spectrum indeed fits the experimental absorption spectrum in an excellent manner for the low-energy region (see Fig. 2). In the higher-energy region the difference between the spectra gives direct access to the higher electronic states. The difference spectrum can be again reasonably fitted by the simulated $1A_g \rightarrow 1B_u$ spectrum, giving evidence that the geometry of the $2B_u$ state is not very different from that of the $1B_u$ state, and contributions of further higher electronic states are negligible. According to the analysis in Fig. 2, the $2B_u$ state is located 4500 cm^{-1} above $1B_u$; the relative oscillator strength being $f_{rel}=f(1A_g \rightarrow 2B_u)/f(1A_g \rightarrow 1B_u)=0.08$. The same analysis was successfully applied to F_{12}DSB, see Fig. 2, leading to a $2B_u-1B_u$ energy difference of 4800 cm^{-1} and $f_{rel}=0.23$.

These data can now be used to determine the relative orientation of the $1A_g \rightarrow 2B_u$ transition from the anisotropy of the fluorescence excitation spectrum (see Fig. 2). The total fluorescence anisotropy r_{tot} in the case of two overlapping absorption bands with contributions x_1 and x_2 is given by

$$r_{tot} = r_1 x_1 + r_2 x_2, \tag{1}$$

where the anisotropy r_i of each contributing band depends on the relative orientation ϑ_i of the absorbing dipole with respect to the emitting dipole,

$$r_i = (3\cos^2 \vartheta_1 - 1) r_0/2. \tag{2}$$

The value of r_0 can be accessed from the anisotropy in the low-energy part of the absorption spectrum where $\vartheta_1=0°$, here $r_0=0.33$ (see Fig. 2). Concomitantly, the relative orientation of the $\mu(1A_g \rightarrow 2B_u)$ transition dipole is determined to be $\vartheta=23°$ against $\mu(1A_g \rightarrow 1B_u)$.

The electronic excitations in the molecules were investigated at the (time-dependent) DFT B3LYP level, using the 6-311G* basis set. The DFT method underestimates the $S_0 \rightarrow S_1$ transition energy of DSB by 4200 cm^{-1}, in contrast to the Hartree-Fock RCIS method, which agrees very well with the experimental value *in vacuo* (see Table II). However, DFT gives reliable results not only for molecular geometries but also for spectral shifts induced by the introduction of substituents: the positive inductive ($+I$) effect of the alkyl substituents, responsible for the redshift of *t*-Bu_4DSB by -400 cm^{-1} against DSB *in vacuo* is in reasonable agreement with the DFT calculations (see Table II). The method also well reproduces the subtle balance between the positive mesomeric ($+M$) effect and the $-I$ effect of the fluorine atoms in F_{12}DSB leading to an overall redshift of -500 cm^{-1} against DSB.

The orientation of the $1A_g \rightarrow 1B_u$ transition of DSB against the long axis of the molecule $d_{\omega\omega'}$ is predicted to be $\gamma=2°$ (see Table II) a value significantly smaller than at a semi-empirical level, $\gamma=8°$.[26] Similar small values of 1°–2° are obtained for the substituted species. For DSB, the $2B_u$ state is calculated to be 9000 cm^{-1} above $1B_u$ at the DFT level, where the transition is oriented in parallel with the $1A_g \rightarrow 1B_u$ transition ($\vartheta=0°$) in agreement with experiment. The relative oscillator strength is calculated to be $f_{rel}=0.006$, one order of magnitude smaller than in experiment. However, the $1A_g \rightarrow 2B_u$ transition may borrow some intensity from the $1A_g \rightarrow 1B_u$ transition. For F_{12}DSB, B3LYP predicts $2B_u$ 6300 cm^{-1} above $1B_u$ and the relative oscillator strength to be $f_{rel}=0.022$. The relative orientation is $\vartheta=33°$ in reasonable agreement with experiment. The different value for ϑ compared to DSB can be rationalized by the asymmetry introduced by the fluorine atoms in the central phenyl ring. While the $1B_u$ state is essentially described by the highest occupied molecular orbital (HOMO) $\rightarrow$ lowest unoccupied molecular orbital (LUMO) ($H \rightarrow L$) excitation with large contributions only at the carbon atoms, the main contribution to the $2B_u$ state is the $H\text{-}2 \rightarrow L$ excitation, where the electronic density in the H-2 orbital is almost exclusively located at the carbon and fluorine atoms of the central phenyl ring.

B. *t*-Bu_4DSB in the solid state

In order to understand the optical and photophysical properties of systems with long-range order of the molecules, it is appropriate to start with disordered materials. Distyrylbenzene with bulky *t*-butyl substitution, *t*-Bu_4DSB, provides an example for solid-state structures without long-range order. This can be shown by measuring the fluorescence anisotropy r_F upon exciting the nanoparticles in the main absorption band. If no energy transfer occurred between the molecules, one would expect the maximum value of $r_F=0.4$ for nanoparticles, randomly distributed in the suspension, due to the absence of rotational motion of the fluorescent molecules.[27] However, in *t*-Bu_4DSB nanoparticles, the fluorescence anisotropy reaches the steady-state value of $r_F=0$, see Fig. 3, within the first 80 ps,[14] thus indicating that the information on molecular orientation is completely lost after a few energy-transfer steps. Concomitantly, the fluorescence spectrum is only slightly redshifted against the solution spectrum (Fig. 3) due to the moderate isotropic polarizability in the disordered system.[28] The relative intensities and energy spacing of the subbands resemble those in solution, indicating that intermolecular vibronic coupling effects are weak in the nanoparticles. The absorption spectrum is only slightly blueshifted against that in solution. Thus, preferential side-by-side orientations, which lead to a strong blueshift of the absorption spectra (H aggregation, *vide infra*), play only a minor role in condensed phases of *t*-Bu_4DSB. However, temporal changes of the absorption spectra on the time scale of several minutes to hours indicate that subtle changes in the molecular arrangements occur, which lead to slightly better ordered domains within the particles.

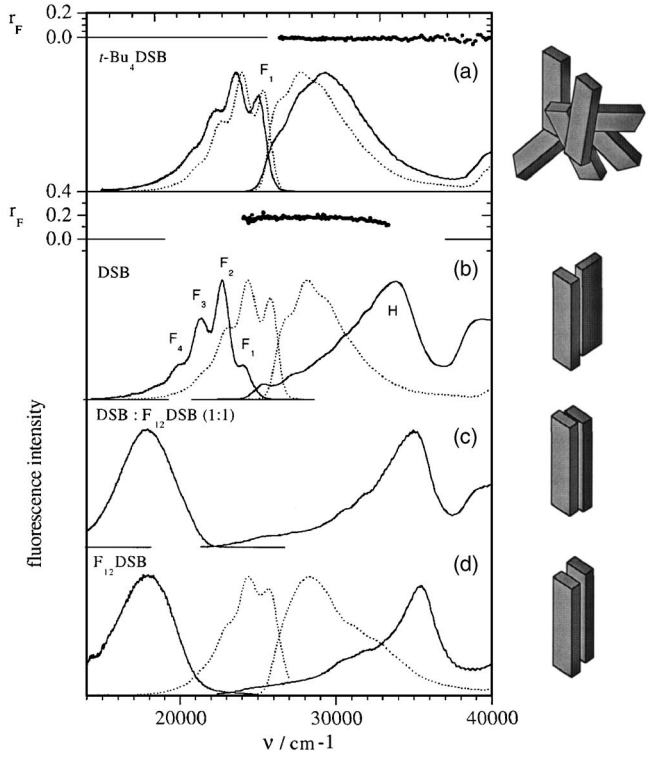

FIG. 3. Fluorescence (left) and absorption spectra (right) of distyrylbenzene nanoparticles: (a) *t*-Bu_4DSB, (b) DSB, (c) cocrystallized DSB:F_{12}DSB, and (d) F_{12}DSB. Spectra in solution (in *n*-hexane; dashed lines) are shown for comparison. Fluorescence excitation anisotropies r_F, recorded at λ_{em} =440 nm, are given for *t*-Bu_4DSB and DSB nanoparticle suspensions. A schematic presentation of the respective condensed-phase structures is given on the right.

C. DSB in the solid state

The solid-state structure of DSB with four molecules per unit cell consists of pin cushion layers of molecules,[1] where the molecules within the layers are organized in a herringbone manner, very similar to the unsubstituted five-ring oligomer[3(a)] and PPV:[4] the long axes of the molecules are oriented in parallel, whereas the inclination angle β between the short axes is around 60° (see Fig. 4). The nearest-neighbor distance in this edge-to-face arrangement can be extracted from the crystallographic data in Ref. 1 to be 4.84 Å, providing medium coupling strength of adjacent molecules within the layer.[29] The long axes of the molecules in adjacent layers are inclined at an angle α of around 130° to each other.[1]

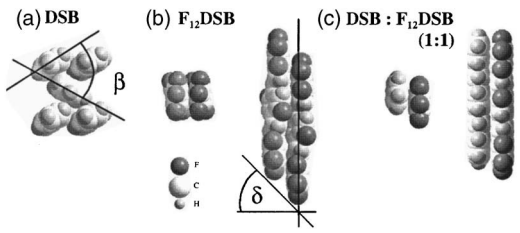

FIG. 4. Arrangement of adjacent molecules within the layers in the solid-state structures. (a) DSB: view along $d_{\omega\omega'}$ (schematic); (b) F_{12}DSB: view along (left) and perpendicular to $d_{\omega\omega'}$ (right); (Ref. 2) (c) cocrystal of DSB:F_{12}DSB (1:1): view along (left) and perpendicular to $d_{\omega\omega'}$ (right) (Ref. 10).

The molecular arrangement in the DSB nanoparticles can be monitored by polarized fluorescence measurements.[28] Upon excitation of the nanoparticles in the main absorption band, a value of $r_F \approx 0.20$ to 0.23 is observed for the fluorescence anisotropy, (Fig. 3) depending on the sample.[13–15,28] This value is the result of averaging of emission polarization by transfer of the excitation energy between translationally nonequivalent molecules on a time scale which is much shorter than the fluorescence lifetime of the sample. Since the long axes $d_{\omega\omega'}$ of the molecules—and therefore the transition dipole moments $\mu(S_0 \rightarrow S_1)$—within the layers are oriented almost in parallel, one can assume just two kinds of translationally nonequivalent transition dipole moments in the DSB nanoparticles. Thus, the inclination angle α between the transition dipole moments of the nonequivalent molecules can be calculated from the observed fluorescence anisotropy by

$$r_F = r_0 \frac{1 + 3\cos^2 \alpha}{4}. \tag{3}$$

Inserting $r_F \approx 0.20-0.23$, an angle α of 125° to 131° between the molecules is calculated, in good agreement with the value of α obtained from the x-ray data, thus confirming that the structure of the nanoparticles is very similar to the one of the single crystal.

Due to the close contact of neighboring molecules in the herringbone layers, the electronic interaction within the layers is much stronger than between the layers. The almost parallel alignment of the $S_0 \leftrightarrow S_1$ molecular transition moments of the molecules in the layer causes a strong blueshift of the main absorption band (H-type aggregation,[30] see Fig. 3), which is well reproduced by quantum-chemical calculations.[26,31] The nature of the electronic excitation can be elucidated by considering the electron-hole two-particle wave functions for the respective state in nearest-neighbor dimer configurations. This analysis allows to determine the charge-transfer character of a given electronic transition due to contributions of interchain excitations. The probability $P_{p,q}$ to find an electron e^- at site p and a hole h^+ at site q is given by[32]

$$P_{p,q} = \frac{|\Psi(p,q)|^2}{\sum_p \sum_q |\Psi(p,q)|^2}, \tag{4}$$

$$\Psi(p,q) = \sum_i C_i c_p(e^-) c_q(h^+), \tag{5}$$

where C_i is the CI coefficient of the excitations i between MOs involved in the description of the excited state, and $c_p(e^-)$ and $c_q(h^+)$ are the linear combination of atomic orbitals (LCAO) coefficients associated with the unoccupied and occupied MOs, respectively. In the edge-to-face dimer arrangement of DSB in the crystal,[22] the S_1 state of the monomer splits into a lower symmetry-forbidden state S_1' and a symmetry-allowed S_2', located around 1800 cm^{-1} above S_1', see Table III. Figure 5(a) shows the probability on a logarithmic scale, $\log(P_{p,q})$, for S_2', as obtained by semiempirical ZINDO/S calculations: high probabilities are found exclusively in the first and third quadrants, which are related to

TABLE III. Lowest excited states of nearest-neighbor dimer configurations of DSB, F_{12}DSB, and DSB:F_{12}DSB crystal structures, obtained at the semiempirical ZINDO/S level: vertical transition energies $\nu_{vert}(\times 1000\ cm^{-1})$, oscillator strengths f, CI coefficients (only contributions >10% are shown), and contributions of interchain excitation (c.s.=charge separation).

Crystal	Dimer configuration	State	$\nu_{vert}(f)$	CI description	Contribution of interchain excitation
DSB	Edge to face	S_1'	27.8 (0.01)	$H\text{-}1 \rightarrow L(-0.45)$	0%
				$H \rightarrow L+1(0.43)$	
		S_2'	29.6 (4.20)	$H\text{-}1 \rightarrow L(0.40)$	0%
				$H \rightarrow L+1(0.41)$	
F_{12}DSB	Face to face	S_1'	27.4 (0.00)	$H\text{-}1 \rightarrow L(0.48)$	2%
				$H \rightarrow L+1(0.40)$	
		S_2'	29.0 (3.60)	$H \rightarrow L(0.69)$	10%
				$H\text{-}1 \rightarrow L+1(0.16)$	
DSB:F_{12}DSB	Face to face	S_1'	25.3 (0.42)	$H \rightarrow L(0.79)$	65% (c.s.)
		S_2'	27.8 (0.14)	$H \rightarrow L+2(0.35)$	30% (c.s.)
				$H\text{-}1 \rightarrow L(0.31)$	
				$H \rightarrow L(0.13)$	
		S_3'	30.0 (3.22)	$H\text{-}1 \rightarrow L(0.27)$	24% (c.s.)
				$H \rightarrow L+2(0.21)$	
				$H\text{-}2 \rightarrow L(0.20)$	
				$H \rightarrow L+1(0.18)$	
		S_4'	30.2 (0.41)	$H \rightarrow L+1(0.37)$	64% (c.s.)
				$H \rightarrow L+2(0.25)$	
				$H\text{-}2 \rightarrow L(0.13)$	
				$H\text{-}1 \rightarrow L(0.12)$	

intrachain excitations. Thus, no contributions of interchain excitations are observed in the herringbone arrangement. Very similar probability patterns are obtained for the displaced face-to-face neighbors in the crystallographic *a* and *b* directions, where the large intermolecular separations (a=5.873 Å, b=7.697 Å) (Ref. 2) prevent interchain contributions to the electronic excitation.

The decrease of the fluorescence quantum yield from Φ_F=0.77 in solution to Φ_F=0.1 in the nanoparticles, see Table I, is caused partly by the decrease of the radiative rate constant due to H aggregation, but also by the existence of nonemissive traps in the condensed phase, which are abundant in nanoparticles, where structural inhomogeneities are expected to be quite common. Thus, in DSB single crystals with low defect concentrations, Φ_F becomes as high as 65%.[1] A similarly high value for Φ_F is obtained by cooling the nanoparticle suspension to T=20 K.[33] The increase of Φ_F with decreasing temperature is caused by the reduction of the rate constant for S_1 energy migration due to the decrease of the spectral overlap between absorption and emission.[34] The emission spectrum of the DSB nanoparticles is redshifted against the solution spectrum by $-1800\ cm^{-1}$ (Fig. 3), due to the high anisotropic polarizability in the particles caused by the preferential orientation of the molecules within the layer.[28] The intensity of the F_1 subband is low, an effect which is ascribed to the electronic coupling of the molecules.[31] Note that the F_1 replica almost vanishes in the low-temperature fluorescence spectrum of the DSB single crystal,[35] due to a very small component of the $\mu(S_0 \rightarrow S_1)$ transition dipole moment vertical to the long molecular axis. The higher intensity of the F_1 band in the nanoparticle spectrum therefore gives further evidence for a higher content of structural inhomogeneities in the nanoparticles.[31] The energy spacing and relative intensities of the F_i replica with $i>1$ (Fig. 3) follow the characteristics of the corresponding fluorescence subbands in solution. This becomes obvious in comparing well-resolved low-temperature spectra of DSB single crystals[35] and solid solutions.[24] Here the vibronic fine structure is almost identical. This clearly indicates that the edge-to-face arrangement of the adjacent molecules in the herringbone layers does not permit strong *intermolecular* vibronic coupling. This can be rationalized by the negligible contribution of interchain excitations to the electronic transition: upon excitation no substantial changes in the intermolecular arrangements are expected which are a prerequisite for intermolecular vibronic coupling.

D. F_{12}DSB in the solid state

The packing motif of F_{12}DSB in the solid state is distinctly different from DSB: The fluorosubstituents promote π-stacking of the oligomers due to interactions of the local carbon-fluorine dipole moments,[2,8,9,36] hence a cofacial arrangement of adjacent F_{12}DSB molecules is found,[2] with an interplane distance of d=3.33 Å. The molecules are slightly shifted along their long molecular axes by 3.45 Å, the "pitch angle," as defined by Curtis *et al.*,[8] being δ=46° (Fig. 4). Two translationally nonequivalent molecules (*A* and *B*) are found in the unit cell, thus a layered structure of cofacially oriented molecules is obtained (see Fig. 6). The colatitude ϕ_i of the long molecule axis (and thus of the $S_0 \leftrightarrow S_1$ transition dipole moment) with respect to the crystallographic *c* axis is

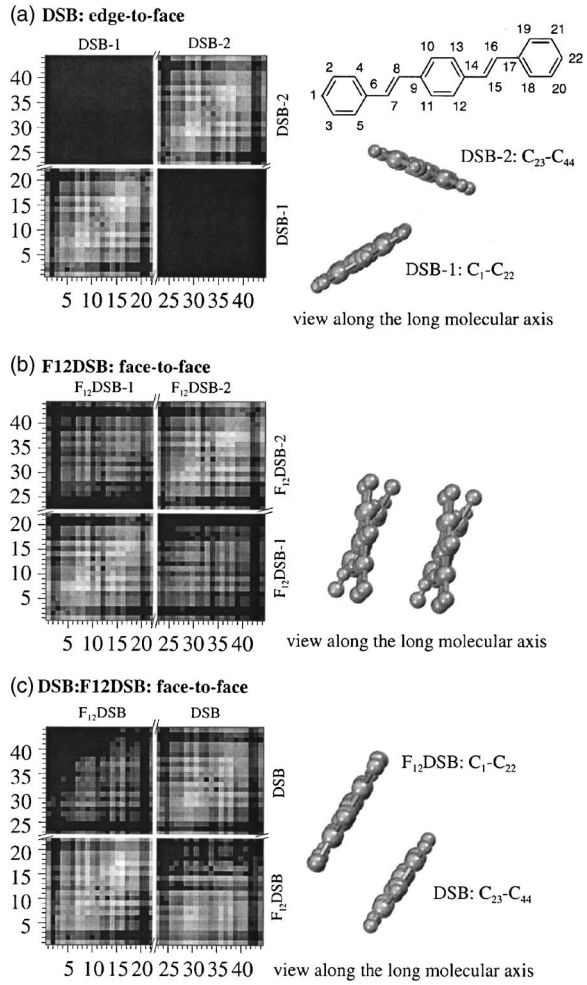

FIG. 5. Electron-hole two-particle wave-function analysis of nearest-neighbor dimer pair configurations in the crystal structure of (a) DSB (edge to face), (b) F_{12}DSB (face to face), and (c) DSB:F_{12}DSB (face to face). Abscissa: position of h^+ at site i. Ordinate: position of e^- at site i. White areas present regions of high probabilities $\log(P_{p,q})$.

$\phi_A=\phi_B=56°$ and the inclined azimuth angle between the molecules A and B is $\theta_{AB}=125°$ (see Fig. 6). The molecular orientation of the molecules with respect to the crystal axes can be monitored by angular-resolved polarized fluorescence spectroscopy. For this purpose the needle-shaped single crystal of F_{12}DSB is irradiated by light polarized in parallel (p) with the long crystal axis (c), and polarized fluorescence is detected parallel (I_{pp}) and perpendicular (I_{ps}) to c (see inset of Fig. 7). In order to calculate the dichroic ratio $D=I_{pp}/I_{ps}$ the intensities are written as a function of the spherical coordinates θ_i, ϕ_i of each molecule $i(A,B)$. Here, fast energy transfer between the individual molecules i within their fluorescence lifetime is taken into account,[37]

$$I_{PP}=\sum_i \cos^2\phi_i \sum_i \cos^2\phi_i, \tag{6}$$

$$I_{ps}=\sum_i \cos^2\phi_i \sum_i \sin^2\phi_i \cos^2\theta_i. \tag{7}$$

Inserting ϕ_A, ϕ_B, $\theta_B=(\theta_A+\theta_{AB})$, and $\theta_A=\theta+\theta_0$, where θ is the angle of rotation around the crystal c axis (see inset of Fig. 7) and θ_0 accounts for the unknown position of the

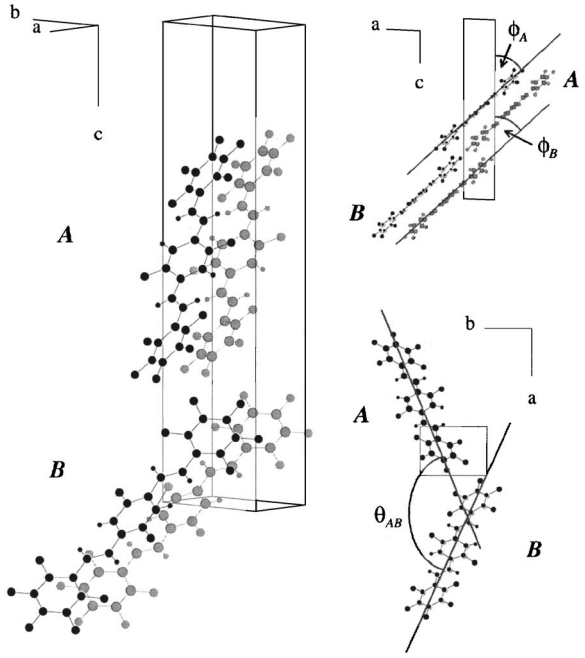

FIG. 6. Representation of the monoclinic unit cell ($P2_{1/c}$) of F_{12}DSB single crystals (Ref. 2). Cell parameters are $a=4.83$ Å, $b=6.64$ Å, $c=28.02$ Å, and $\beta=92.3°$. The two translationally nonequivalent molecules in the unit cell are indicated (A,B).

molecules A and B with respect to the x and y axes of the laboratory coordinate system, the calculated curve, given as solid line in Fig. 7, is obtained, in good agreement with the measured data, given as solid symbols in the graph.

The parallel orientation of the transition dipoles of adjacent molecules within the layers again causes H aggregation (see Fig. 3). The blueshift of the absorption band in F_{12}DSB nanoparticles is larger compared to that of DSB, indicating a stronger overall electronic interaction of the F_{12}DSB mol-

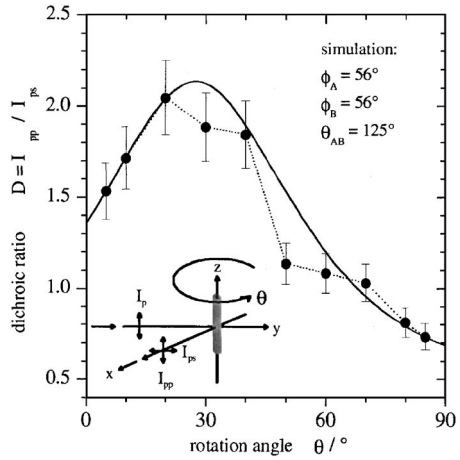

FIG. 7. Dichroic ratio of fluorescence $D=I_{pp}/I_{ps}$ of a F_{12}DSB single crystal as a function of the rotation angle θ (the parameters used are defined in the inset). Closed symbols: experimental values ($\lambda_{excitation}=370$ nm, $\lambda_{emission}=477$ nm) with 10% error bars; solid line: theoretical curve, obtained from the positions of the molecules in the unit cell, according to x-ray data, and the orientation of the transition dipole moment $\mu(S_0\leftrightarrow S_1)$ with respect to the geometry of the molecule, according to quantum-chemical calculations. The inserted variables are $\phi_A=\phi_B=56°$, $\theta_{AB}=125°$, and $\theta_0=90°$ (for definitions see text).

ecules. The radiative rate constant $k_F=\Phi_F/\tau_F=10^6$ s^{-1} (Table I) is more than two orders of magnitudes smaller than in solution, due to the dipole forbidden nature of the transition between the ground state and the lower exciton state of the crystal.

In stark contrast to DSB, the F_{12}DSB emission spectrum is unstructured and strongly redshifted against the one in solution (see Fig. 3). In a former joint experimental and theoretical study on a covalently linked dimer of cofacially oriented stilbene units,[38] we have shown that this kind of excimerlike emission originates from strong intermolecular vibronic coupling of interplane breathing modes to the electronic transition. The high FC activity of these modes stems from the decrease of the intermolecular distance upon electronic excitation. In order to investigate if this is also the case for the excimerlike fluorescence in the F_{12}DSB crystal, ZINDO/S calculations for the face-to-face configuration were performed: the symmetry allowed S_2' state for the cofacial dimer pair is located around 1700 cm^{-1} above the forbidden S_1' state (Table III), where the two states arise from the S_1 states of the respective monomers. The electron-hole two-particle wave-function analysis of the S_2' state is given in Fig. 5(b). The intensities in the second and fourth quadrants, which are due to interchain excitations, amount to 10% of the overall probability distribution. The substantial charge-transfer character of the electronic transition is expected to cause a significant change of the intermolecular separation, thus indeed allowing for efficient intermolecular electron-phonon coupling in the crystal. In contrast, the next neighbor pairs, i.e., edge-to-edge dimers, do not show any contributions of interchain excitations for the lowest allowed excited state. A relevant charge-transfer character of the main electronic transition in the F_{12}DSB crystal is therefore predicted only along the π-stacks.

The 1:1 binary crystal of DSB and F_{12}DSB exhibits also a cofacial arrangement, slipped along the short molecular axis ("rolled" π-stack[8]), with an interplane distance of 3.36 Å (see Fig. 4).[10] Since the arrangement as well as the intermolecular distances are not very different in DSB:F_{12}DSB and F_{12}DSB nanoparticles, the absorption and emission profiles are very similar, showing H-type absorption and excimerlike emission (see Fig. 3). However, the electron-hole two-particle wave-function analysis reveal subtle differences. The lowest excited states cannot be simply described by the splitting of the S_1 states of the respective monomers, but show a distinct mixing of different electronic levels (see Table III). The generated first four excited states have nonzero transition dipole moments and show strong contributions of interchain excitation. Figure 5(c) depicts the $\log(P_{p,q})$ distribution for the most intense S_3' state: interchain contributions are mainly located in the fourth quadrant, therefore charge separation between the chains takes place upon electronic excitation, shifting electron density from DSB to F_{12}DSB.

IV. CONCLUSIONS

Distyrylbenzenes (DSB, F_{12}DSB, and t-Bu_4DSB) were investigated in dilute solutions, nanoparticle suspensions, and single crystals by absorption and polarized fluorescence spectroscopy in order to elucidate the consequences of the intermolecular arrangement on the optical and photophysical properties. The absorption and fluorescence spectra of all molecules in solution are quite similar. Subtle differences of t-Bu_4DSB and F_{12}DSB against DSB in the energies, intensities, and orientations of the transitions to the first and second allowed excited states were clarified by quantum-chemical calculations. Due to the small differences of the constituent molecules, the differences of the optical properties in the solid state are essentially caused by different intermolecular organization. t-Bu_4DSB does not show a long-range order of the constituting molecules. Concomitantly, the properties are very similar to solution. DSB organizes in layer with an edge-to-face arrangement of the molecules (herringbone), whereas F_{12}DSB as well as DSB:F_{12}DSB cocrystals organize in layers of face-to-face oriented molecules (π-stacks). The layered structures with preferential parallel orientation of the molecular $S_0\rightarrow S_1$ transition dipole moments promote H aggregation for DSB as well as for F_{12}DSB and DSB:F_{12}DSB; strongly blueshifted absorption spectra and low radiative rate constants are observed. The emission properties are significantly different: herringbone structures show well-resolved spectra, very similar to solution, thus no significant contribution of intermolecular vibronic coupling is present. In the π-stack structures a significant charge-transfer character of the electronic transition is found, which is expected to induce efficient coupling of intermolecular vibrational modes. The high Franck-Condon activities of these modes are responsible for the strongly redshifted, unstructured excimerlike emission spectra in π-stack arrangements.

ACKNOWLEDGMENTS

The work in Tübingen and Mons was supported by the European Commission through the Human Potential Programme (RTN NANOCHANNEL, Grant No. HRPN-CT-2002-00323). The t-butyl substituted distyrylbenzene was provided by K. Müllen, MPI Mainz (Germany). One of the authors (J.G.) thanks Jochen Glaser, Tübingen (Germany), for helpful discussions. One of the authors (D.B.) is a research associate of the Belgian National Fund for Scientific Research (FNRS).

[1] C. C. Wu, M. C. DeLong, Z. V. Vardeny, J. P. Ferraris, and J. J. Gutierrez, Synth. Met. **137**, 939 (2003); C. C. Wu, O. J. Korovyanko, M. C. DeLong, Z. V. Vardeny, J. J. Gutierrez, and J. P. Ferraris, Synth. Met. **139**, 735 (2003).
[2] M. L. Renak, G. P. Bartholomew, S. Wang, P. J. Ricatto, R. J. Lachicotte, and G. C. Bazan, J. Am. Chem. Soc. **121**, 7787 (1999).
[3] P. F. van Hutten, J. Wildemann, A. Meetsma, and G. Hadziioannou, J. Am. Chem. Soc. **121**, 5910 (1999); S. Vaday, H. C. Geiger, B. Cleary, J. Perlstein, and D. G. Whitten, J. Phys. Chem. B **101**, 321 (1997).
[4] T. Granier, E. L. Thomas, D. R. Gagnon, F. E. Karasz, and R. W. Lenz, J. Polym. Sci., Part B: Polym. Phys. **24**, 2793 (1986).
[5] L. Antolini, G. Horowitz, F. Kouki, and F. Garnier, Adv. Mater. (Weinheim, Ger.) **10**, 382 (1998); T. Siegrist, C. Kloc, R. A. Laudise, H. E. Katz, and R. C. Haddon, Adv. Mater. (Weinheim, Ger.) **10**, 379 (1998).
[6] K. N. Baker, A. V. Fratini, T. Resch, H. C. Knachel, W. W. Adams, E. P. Socci, and B. L. Farmer, Polymer **34**, 1571 (1993).
[7] D. Holmes, S. Kumaraswamy, A. J. Matzger, and K. P. C. Vollhardt, Chem.-Eur. J. **5**, 3399 (1999).
[8] M. D. Curtis, J. Cao, and J. W. Kampf, J. Am. Chem. Soc. **126**, 4318 (2004).

[9] Y. Sakamoto, S. Komatsu, and T. Suzuki, J. Am. Chem. Soc. **123**, 4643 (2001); J. A. R. P. Sarma and G. R. Desiraju, Acc. Chem. Res. **19**, 222 (1986).
[10] G. P. Bartholomew, X. Bu, and G. C. Bazan, Chem. Mater. **12**, 2311 (2000).
[11] A. Camerman and J. Trotter, Acta Crystallogr. **18**, 636 (1965); A. C. Hazell, F. K. Larsen, and M. S. Lehmann, Acta Crystallogr., Sect. B: Struct. Crystallogr. Cryst. Chem. **28**, 2977 (1972).
[12] D. Horn and J. Rieger, Angew. Chem., Int. Ed. **40**, 4330 (2001); H. Kasai, H. S. Nalwa, S. Okada, H. Oikawa, and H. Nakanishi, in *Handbook of Nanostructured Materials and Nanotechnology*, edited by H. S. Nalwa (Academic, New York, 2000), Vol. 5, Chap. 8, pp. 4330–4361; H. Nakanishi and H. Oikawa, in *Single Organic Nanoparticles*, edited by H. Masuhara, H. Nakanishi, and K. Sasaki (Springer, New York, 2003), pp. 17–31.
[13] J. Gierschner and D. Oelkrug, in *Encyclopedia of Nanoscience and Nanotechnology*, edited by H. S. Nalwa (American Scientific Publishers, Stevenson Ranch, CA, 2004), Vol. 8, pp. 219–238.
[14] H.-J. Egelhaaf, J. Gierschner, and D. Oelkrug, Synth. Met. **83**, 221 (1996).
[15] D. Oelkrug, H.-J. Egelhaaf, J. Gierschner, and A. Tompert, Synth. Met. **76**, 249 (1996); J. Gierschner, H.-J. Egelhaaf, and D. Oelkrug, Synth. Met. **84**, 529 (1997); D. Oelkrug, A. Tompert, J. Gierschner, H.-J. Egelhaaf, M. Hanack, M. Hohloch, and E. Steinhuber, J. Phys. Chem. B **102**, 1902 (1998).
[16] A. E. Siegrist, P. Liechti, H. R. Meyer, and K. Weber, Helv. Chim. Acta **52**, 2521 (1969).
[17] R. Erckel and H. Frühbeis, Z. Naturforsch. B **37**, 1472 (1982).
[18] R. Schenk, H. Gregorius, K. Meerholz, J. Heinze, and K. Müllen, J. Am. Chem. Soc. **113**, 2634 (1991).
[19] R. Ahlrichs, M. Bär, H.-P. Baron *et al.*, computer code TURBOMOLE version 5.7.1 (Universität Karlsruhe, Karlsruhe, 2003).
[20] M. J. Frisch, G. W. Trucks, H. B. Schlegl *et al.*, computer code GAUSSIAN 98, revision A.7 (Gaussian, Inc., Pittsburgh, PA, 1998).
[21] M. C. Zerner, in *Reviews in Computational Chemistry*, edited by K. W. Lipkowitz and D. B. Boyd (VCH, New York, 1994), Vol. 2, p. 313.
[22] The edge-to-face molecular arrangement of DSB was constructed from the crystallographic data in Ref. 1. The inclination between the short axes were assumed to $\beta=60°$ in analogy to similar structures (Refs. 3–5), and the one between the long axes was estimated from Ref. 1 to $\alpha=130°$. The geometry of DSB was optimized at the B3LYP/6-311G* level of theory.
[23] T. Damerau and M. Hennecke, J. Chem. Phys. **103**, 6232 (1995).
[24] J. Gierschner, H.-G. Mack, L. Lüer, and D. Oelkrug, J. Chem. Phys. **116**, 8596 (2002).
[25] L. Onsager, J. Am. Chem. Soc. **58**, 1486 (1936).
[26] F. C. Spano and S. Siddiqui, Chem. Phys. Lett. **314**, 481 (1999); F. C. Spano, J. Chem. Phys. **114**, 5376 (2001).
[27] Fluorescence depolarization due to the rotation of the nanoparticles in the suspension can be excluded, since the rotational diffusion of the particles (diameter around 100 nm) is much slower than the lifetime of fluorescence.
[28] H.-J. Egelhaaf, J. Gierschner, and D. Oelkrug, Synth. Met. **127**, 221 (2002).
[29] J. Cornil, D. A. dos Santos, X. Crispin, R. Silbey, and J. L. Brédas, J. Am. Chem. Soc. **120**, 1289 (1998).
[30] R. M. Hochstrasser and M. Kasha, Photochem. Photobiol. **3**, 317 (1964); M. Kasha, H. R. Rawls, and M. A. El-Bayoumi, Pure Appl. Chem. **11**, 371 (1965).
[31] F. C. Spano, J. Chem. Phys. **116**, 5877 (2002); F. C. Spano, J. Chem. Phys. **118**, 981 (2003); F. C. Spano, J. Chem. Phys. **120**, 7643 (2004).
[32] J. Rissler, J. H. Bässler, F. Gebhard, and P. Schwerdtfeger, Phys. Rev. B **64**, 045122 (2001); E. Zojer, P. Buchmacher, F. Wudl, J. Cornil, J. P. Calbert, J.-L. Brédas, and G. Leising, J. Chem. Phys. **113**, 10002 (2000).
[33] K.-H. Schweikhart, M. Hohloch, E. Steinhuber, M. Hanack, L. Lüer, J. Gierschner, H.-J. Egelhaaf, and D. Oelkrug, Synth. Met. **121**, 1641 (2001).
[34] J. Gierschner, H.-J. Egelhaaf, and D. Oelkrug (unpublished).
[35] C. C. Wu, E. Ehrenfreund, J. J. Gutierrez, J. P. Ferraris, and Z. V. Vardeny, Phys. Rev. B **71**, 081201 (2005).
[36] R. Capelli, M. A. Loi, C. Taliani, H. B. Hansen, M. Muria, G. Ruani, M. Muccini, P. W. Lovenich, and W. J. Feast, Synth. Met. **139**, 909 (2003).
[37] In the case where no energy transfer (ET) between the molecules is present, Eqs. (4) and (5) read

$$I_{\mathrm{pp}} = \sum_i \cos^4 \phi_i,$$

$$I_{\mathrm{ps}} = \sum_i \cos^2 \phi_i \sin^2 \phi_i \cos^2 \theta_i.$$

If the colatitudes ϕ_i of the molecules are identical, e.g., in F_{12}DSB, the resulting equations for the dichroic ratio are the same, both with and without ET.
[38] J. Gierschner, H.-G. Mack, D. Oelkrug, I. Waldner, and H. Rau, J. Phys. Chem. A **108**, 257 (2004).